ADVANCED MATERIALS

hensive review see Z. L. Wang, Z. C. Kang, *Functional and Smart Materials—Structural Evolution and Structure Analysis*, Plenum Press, New York **1998**, Ch. 4). These oxides were formed by introducing ordered oxygen vacancies in the fluorite-based unit, but the fcc cation sublattice is a superstable frame, which is independent of the distribution of oxygen vacancies.
[11] K. Otsuka, Y. Wang, E. Sunada, I. Yamanaka, *J. Catal.* **1998**, *175*, 152.
[12] J. P. Schaffer, A. Saxena, S. D. Antolovich, T. H. Sanders, S. B. Warner, *The Science and Design of Engineering Materials*, 2nd ed., McGraw-Hill, New York **1997**, Appendix B.
[13] Oxidation of CO is usually carried out using a metal catalyst such as Pt, see D. C. Skelton, R. G. Tobin, D. K. Lambert, C. L. DiMaggio, G. B. Fisher, *J. Phys. Chem. B* **1999**, *103*, 946.
[14] Z. L. Wang, Z. C. Kang, *Functional and Smart Materials—Structural Evolution and Structure Analysis*, Plenum Press, New York **1998**, Ch. 4.
[15] R. E. Ferguson, E. D. Guth, L. Eyring, *J. Am. Chem. Soc.* **1954**, *76*, 3890.
[16] J. M. Honig, A. F. Clifford, P. A. Faeth, *Inorg. Chem*. **1963**, *2*, 791.
[17] R. G. Haore, L. Eyring, *Handb. Phys. Chem. Rare Earths* **1994**, *18*, 413.
[18] B. G. Hyde, D. J. M. Bevan, L. Eyring, *Philos. Trans. R. Soc. London, A* **1966**, *259*, 583.
[19] J. Kordis, L. Eyring, *J. Phys. Chem*. **1968**, *72*, 2030.
[20] J. Kordis, L. Eyring, *J. Phys. Chem*. **1968**, *72*, 2044.

Quantum Confinement Observed in ZnO/ZnMgO Nanorod Heterostructures**

By *Won Il Park*, *Gyu-Chul Yi*,* *Miyoung Kim*, and *Stephen J. Pennycook*

One-dimensional nanostructures, including nanotubes, nanowires, and nanorods, are potentially ideal functional components for nanometer-scale electronics and optoelectronics.[1–3] Homogeneous carbon nanotubes and nanowires have already been employed in various nanoscale devices.[4–6] However, the ability to fabricate nanoscale heterostructures with well-defined crystalline interfaces opens up many new device applications, as already proven in thin-film semiconductor electronics and photonics.[7] In particular, embedding quantum structures in a single nanorod would enable novel physical properties such as quantum confinement to be exploited, for example, the continuous tuning of spectral wavelength by varying the well thickness. Here, we report the catalyst-free fabrication of quantum-well nanorod heterostructures that exhibit atomically abrupt interfaces and a well-width dependent blue shift resulting from quantum confinement. The ability to grow tunable quantum-well heterostructure nanorods is expected to greatly increase the versatility and power of these building blocks for applications in nanoscale photonics and electronics.

Quantum confinement effects in heterostructure nanowires or nanorods have not been clearly observed despite the recent synthesis of compositionally modulated nanowire superlattices by the vapor–liquid–solid (VLS) growth process.[8–10] This may result from the relatively broad heterostructure interfaces caused by re-alloying of alternating reactants in the metal catalyst during the condensation–precipitation process.[8] In that case, abrupt interfaces would be expected using a non-catalytic growth technique to minimize the formation of a mixed interfacial layer,[11] i.e., by utilizing direct adsorption of atoms on the top surface of nanorods. Nanoscale heterostructures can then be formed by direct epitaxial growth using the techniques already developed for growth of thin-film heterostructure devices. In this paper, we demonstrate this to be the case by the fabrication of quantum-well structures within individual nanorods. With precise thickness control down to the monolayer level, these heterostructures show the clear signature of quantum confinement, an increasing blue-shift with decreasing layer thickness, which is in good agreement with theoretical predictions.

Our approach to fabricating heterostructure nanorods utilizes metal–organic vapor phase epitaxy (MOVPE) to grow high-quality ZnO nanorods,[11] thus eliminating the metal catalyst usually required in other methods.[12] To fabricate heterostructures within the nanorods, $Zn_{1-x}Mg_xO$ ($x < 0.3$) alloy was employed since it has a lattice mismatch with ZnO of less than 1 % as well as a larger bandgap.[13] ZnO nanorods were first prepared on $Al_2O_3(00{\cdot}1)$ substrates using MOVPE.[11] Nanorods are formed as a result of preferential growth along the *c*-axis of ZnO, offering an ideal method for fabrication of nanoscale heterostructures. By introducing Mg precursor into the reactor, $Zn_{1-x}Mg_xO$ layers were epitaxially grown only on the tips of the ZnO nanorods. This growth method ensures minimal intermixing, since no dissolution is required in a catalyst particle, and creates sharp interfaces that enable a wide family of structures and devices to be fabricated.

The multiple quantum well (MQW) nanorods prepared in this study consist of 10 periods of $Zn_{0.8}Mg_{0.2}O$/ZnO on ZnO nanorods (a schematic diagram of the MQW nanorods is shown in Fig. 1A). For ZnO nanorod growth, we employed diethylzinc (DEZn) and oxygen as the reactants with argon as the carrier gas. Details of the ZnO nanorod growth are described elsewhere.[11] For $Zn_{1-x}Mg_xO$ growth bis(cyclopentadienyl)magnesium (Cp_2Mg) was used as the Mg precursor, with composition controlled through the partial pressure.[13] The growth time for the ZnMgO barrier layers was fixed at 36 s, while growth times for the ZnO well layers were set at 12, 18, and 27 s, resulting in well widths of 1.1, 1.7, and 2.5 nm, respectively, as determined by transmission electron microscopy (TEM). The compositions of the $Zn_{1-x}Mg_xO$ layers in the heterostructure and MQW nanorods were determined by energy dispersive X-ray spectroscopy and for all samples x was approximately 0.2.

[*] Prof. G.-C. Yi, W. I. Park
Department of Materials Science and Engineering
Pohang University of Science and Technology (POSTECH)
Pohang, Kyoungbuk 790-784 (Korea)
E-mail: gcyi@postech.ac.kr
Dr. M. Y. Kim
Samsung Advanced Institute of Science and Technology
PO Box 111, Suwon 440-600 (Korea)
Dr. S. J. Pennycook
Oak Ridge National Laboratory
PO Box 2008, Oak Ridge, TN 37831-6030 (USA)

[**] This research was supported by the National Program for Nanostructured Materials Technology of the Ministry of Science and Technology as one of the 21st century Frontier Programs and in part by the Division of Materials Sciences, U.S. Department of Energy, under contract DE-AC05-00OR22725 with Oak Ridge National Laboratory managed by UT-Battelle, LLC. Extensive use of the facilities at POSTECH is acknowledged.

 © 2003 WILEY-VCH Verlag GmbH & Co. KGaA, Weinheim 0935-9648/03/0603-0526 $ 17.50+.50/0

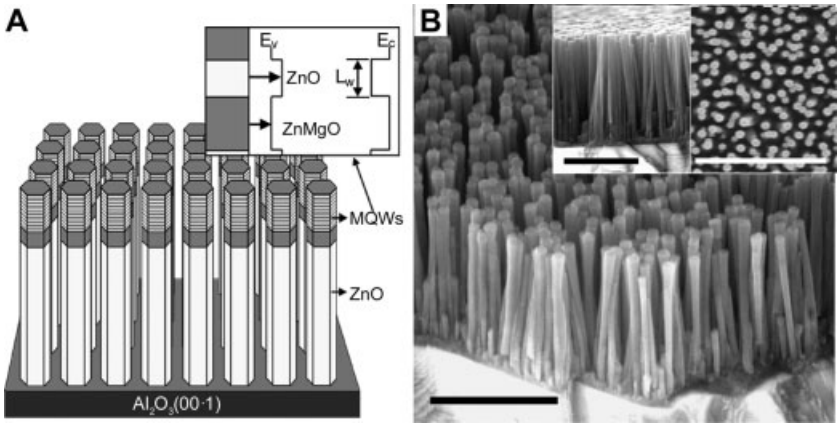

Fig. 1. A) Schematic of multiple quantum well (MQW) nanorods consisting of 10 periods of $Zn_{0.8}Mg_{0.2}O$/ZnO on the tips of ZnO nanorods. An electronic band diagram for the MQW is inset. B) FE-SEM images of the MQW nanorods. Scale bar: 0.5 μm.

Field-emission scanning electron microscopy (FE-SEM) images of the MQW nanorods are shown in Figure 1B, revealing that the nanorods were well aligned vertically with homogeneous length and diameter distributions. Typical mean diameters and lengths were in the range of 20–70 nm and 0.5–2 μm, respectively. Additionally, X-ray diffraction (XRD) results showed that the nanorod heterostructures were epitaxial with homogeneous in-plane alignment as well as *c*-axis orientation along the substrate normal.[11]

Figures 2A and B show TEM images of the samples with 1.1 and 2.5 nm wells, respectively. Both images exhibit bright and dark layers in the MQW, corresponding to the $Zn_{0.8}Mg_{0.2}O$ and ZnO layers, respectively. The interfaces between the different layers are clearly visible. Figure 2C shows a high-resolution TEM image of the 2.5 nm sample. Nanorods grown along the *c*-axis of the hexagonal crystal structure are almost defect-free except for a few edge dislocations. The interfaces between ZnO and $Zn_{0.8}Mg_{0.2}O$ are as clean as the ZnO layer, and interface dislocations are rarely observed, presumably due to the small lattice mismatch.

Z-contrast images of the MQW nanorods are shown in Figures 2D–H. It has been shown over the last decade that scanning TEM (STEM) imaging obtained from a high-angle annular dark field (HAADF) detector can be described as incoherent scattering, referred to as *Z*-contrast imaging, because each column of the image follows approximately the expected Z^2 dependence (where Z is an atomic number) of the Rutherford scattering cross section.[14] Since lighter elements scatter less, ZnO layers are brighter than $Zn_{0.8}Mg_{0.2}O$ layers in a *Z*-contrast image.

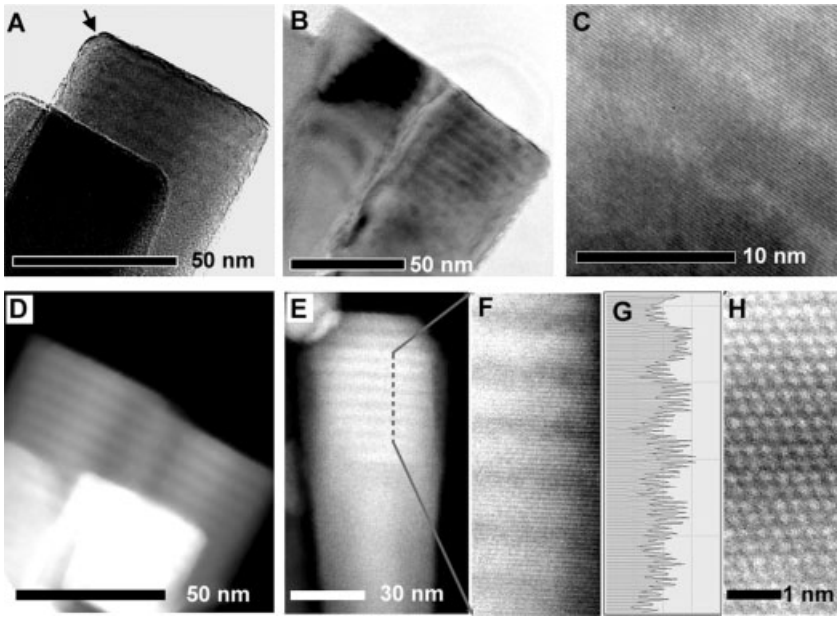

Fig. 2. TEM images of ZnO/$Zn_{0.8}Mg_{0.2}O$ MQW nanorods. A,B) Low-magnification TEM images of the samples with 1.1 and 2.5 nm wells. The repeating dark and bright layers represent the MQW region. C) High-resolution TEM image of the 2.5 nm sample. D–H) *Z*-contrast images of the 2.5 nm sample with increasing magnification and an intensity profile (G) along the dashed line in (E). The *Z*-contrast image clearly shows the compositional variation, with the bright layers representing the ZnO well layers.

In the higher magnification image, Figure 2F, the ZnO lattice is resolved, providing an internal magnification calibration. The MQW period was determined to be 5.5 ± 0.1 nm, close to that expected from the growth times. However, the intensity profile across this image (Fig. 2G) shows that the boundaries between ZnO and $Zn_{0.8}Mg_{0.2}O$ are not very clear. Since ZnO/ZnMgO heterostructures are thermally stable up to 750 °C,[15] interdiffusion during the low temperature growth at 450 °C is expected to be negligible. Furthermore, between each change in composition of the reaction gases the system was purged with pure argon and oxygen, so no layer of mixed composition is expected. We attribute the apparent broadening of the interface to the slightly rounded shape of the nanorod growth surface near the sides of the rod (arrowed in Fig. 2A). In projection, this will lead to an apparent blurring of the interface on the order of 1 nm, as observed. Interestingly, the atomic resolution image, Figure 2H, indicates the presence of a superlattice in both the wells and barrier

 © 2003 WILEY-VCH Verlag GmbH & Co. KGaA, Weinheim 0935-9648/03/0603-0527 $ 17.50+.50/0

ADVANCED MATERIALS

layers, with periodicity equal to the *c*-axis lattice parameter. Its origin is unclear: a composition modulation on the Zn sublattice seems unlikely given the growth conditions, and although O is not imaged directly, a periodic composition modulation on the O sublattice (such as an ordered array of vacancies or impurities) could introduce periodic strains into the Zn sublattice, resulting in the periodic change in columnar intensity.

Figure 3 shows the photoluminescence (PL) spectrum from single heterostructure nanorods measured at 10 K. The dominant PL emission peak at 3.360 eV corresponds to the well-

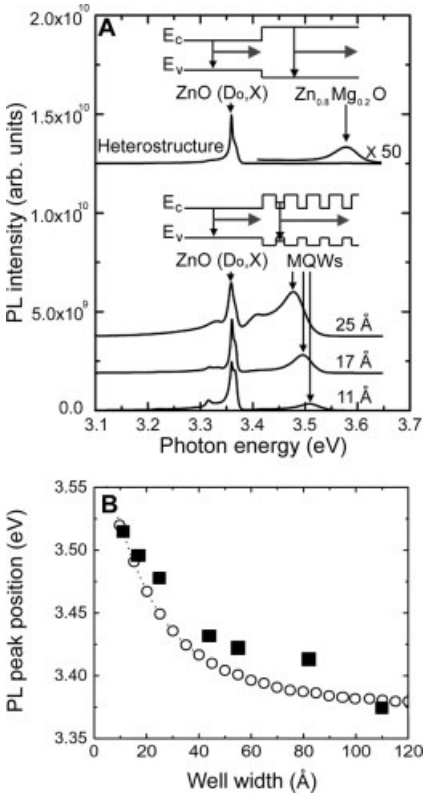

Fig. 3. A) 10 K PL spectra of $ZnO/Zn_{0.8}Mg_{0.2}O$ heterostructure nanorods and $ZnO/Zn_{0.8}Mg_{0.2}O$ MQW nanorods with band diagrams shown inset. B) Well-width dependent PL peak positions in $ZnO/Zn_{0.8}Mg_{0.2}O$ MQW nanorods (squares) and theoretically calculated values (circles) in 10 periods of one-dimensional square potential wells. In this calculation, we employed following parameters; $0.28m_0$ and $1.8m_0$ for the effective masses of electron and hole, respectively, a ratio of conduction and valance band offsets ($\Delta E_c/\Delta E_v$) of 9, and a bandgap offset (ΔE_g) of 250 meV.

known neutral-donor bound excitons (D_o,X) in ZnO.[16,17] No blue-shift in the PL spectrum of ZnO nanorods is observed due to their large lateral size of ~40 nm. In addition to the dominant PL peak, another weak PL peak is seen at 3.58 eV, ascribed to excitonic emission from the single $Zn_{0.8}Mg_{0.2}O$ layer.[13] However, PL spectra of $ZnO/Zn_{0.8}Mg_{0.2}O$ MQW nanorods exhibit new peaks with emission energies dependent on well widths, as indicated by the arrows. PL emission from the 2.5, 1.7, and 1.1 nm MQW nanorods is blue-shifted to 3.478, 3.496, and 3.515 eV, respectively. Results from other samples are included in Figure 3B; the blue-shift decreases with increasing well width and is almost negligible at a well width of 110 Å. Results from theoretical predictions in finite periodic square-well potential are also shown,[18] and it is seen that the systematic increase in PL emission energy with reducing well width is consistent with the quantum confinement effect.

Our controlled heteroepitaxial growth of $ZnO/Zn_{1-x}Mg_xO$ MQW nanorods by MOVPE opens up significant opportunities for the fabrication of quantum device structures on a single nanorod. The simple but accurate thickness control allows heteroepitaxial growth of well-defined potential profiles resulting in nanosized well structures in individual nanorods that are tunable through the effects of quantum confinement. These quantum building blocks may be used as components for nanoscale resonant tunneling devices, field-effect transistors, and light-emitting devices. More generally, we believe that the simple "bottom–up" epitaxial approach might readily be expanded to create many other heteroepitaxial semiconductor nanorods.

Experimental

For the fabrication of $ZnO/Zn_{1-x}Mg_xO$ heterostructure nanorods, ZnO nanorods were prepared on $Al_2O_3(00{\cdot}1)$ substrates using a low-pressure MOVPE system. No metal impurity catalyst was deposited on the substrates. For ZnO nanorod growth, diethylzinc and oxygen were employed as the reactants with argon as the carrier gas [11]. For $Zn_{1-x}Mg_xO$ growth on the ZnO nanorods, *bis*-cyclopentadienyl-Mg was used as the Mg precursor. The composition of the $Zn_{1-x}Mg_xO$ layer was controlled by changing the partial pressure of the Mg precursor [13]. $ZnO/Zn_{1-x}Mg_xO$ superlattice nanorods consisting of 10 periods of $ZnO/Zn_{1-x}Mg_xO$ heterostructures on ZnO nanorods were fabricated by controlling the reactant gas flow directions to either a reactor or vent. The growth times of ZnO well layers in the samples were 12, 18, and 27 s, yielding the well layer widths of 11, 17, and 25 Å, respectively, while a growth time of ZnMgO barrier layers was fixed at 36 s. The compositions of the $Zn_{1-x}Mg_xO$ layers in the heterostructure and superlattice nanorods were determined by energy dispersive X-ray spectroscopy in a transmission electron microscopy chamber. The average concentration of Mg in the ZnMgO layers was about 20 at.-%. The TEM samples were prepared by scratching the film surface, diffusing those pieces inside alcohol, and putting them on carbon films. A Philips 300 kV FE-TEM with 1.7 Å point resolution was used to obtain both the TEM and *Z*-contrast images. Since nanorods tend to lie flat on carbon films, most {0001} nanorod planes exist in the Bragg condition. The PL measurements were performed at 10 K with an optical resolution of 0.05 nm and the 325 nm line of a He-Cd laser, described elsewhere [16].

Received: October 21, 2002

[1] C. Dekker, *Phys. Today* **1999**, *52(5)*, 22.
[2] J. Hu, T. W. Odom, C. M. Lieber, *Acc. Chem. Res.* **1999**, *32*, 435.
[3] J. T. Hu, L. Li, W. Yang, L. Manna, L. Wang, A. P. Alivisatos, *Science* **2001**, *292*, 2060.
[4] S. J. Tans, A. R. M. Verschueren, C. Dekker, *Nature* **1998**, *393*, 49.
[5] X. Duan, Y. Huang, Y. Cui, J. Wang, C. M. Lieber, *Nature* **2001**, *409*, 66.
[6] J. Wang, M. S. Gudiksen, X. Duan, Y. Cui, C. M. Lieber, *Science* **2001**, *293*, 1455.
[7] C. Weisbuch, B. Vinter, *Quantum Semiconductor Structures: Fundamentals and Applications*, Academic, San Diego, CA **1991**.
[8] M. S. Gudiksen, L. J. Lauhon, J. Wang, D. C. Smith, C. M. Lieber, *Nature* **2002**, *415*, 617.
[9] Y. Wu, R. Fan, P. Yang, *Nano Lett.* **2002**, *2*, 83.
[10] M. T. Bjork, B. J. Ohlosson, T. Sass, A. I. Persson, C. Thelander, M. H. Magnusson, K. Deppert, L. R. Wallenberg, L. Samuelson, *Nano Lett.* **2002**, *2*, 87.
[11] W. I. Park, D. H. Kim, S.-W. Jung, G.-C. Yi, *Appl. Phys. Lett.* **2002**, *80*, 4232.

 © 2003 WILEY-VCH Verlag GmbH & Co. KGaA, Weinheim 0935-9648/03/0603-0528 $ 17.50+.50/0

[12] M. H. Huang, S. Mao, H. Feick, H. Yan, Y. Wu, H. Kind, E. Weber, R. Russo, P. Yang, *Science* **2001**, *292*, 1897.
[13] W. I. Park, G.-C. Yi, H. M. Jang, *Appl. Phys. Lett.* **2001**, *79*, 2022.
[14] S. J. Pennycook, D. E. Jesson, *Ultramicroscopy* **1991**, *37*, 14.
[15] A. Ohtomo, R. Shiroki, I. Ohkubo, H. Koinuma, M. Kawasaki, *Appl. Phys. Lett.* **1999**, *75*, 4088.
[16] S. W. Jung, W. I. Park, H. D. Cheong, G.-C. Yi, H. M. Jang, S. Hong, T. Joo, *Appl. Phys. Lett.* **2002**, *80*, 1924.
[17] G. Reynolds D. C. Reynolds, D. C. Look, B. Jogai, *Phys. Rev. B* **1998**, *57*, 12 151.
[18] S. L. Chuang, in *Physics of Optoelectronic Devices* (Eds: J. W. Goodman), Wiley, New York **1995**, Ch. 4.

Stable Nanoporous Metallic Nickel Colloids**

By *Yoshiyuki Hattori*, *Takehisa Konishi*, *Hirofumi Kanoh*, *Shinji Kawasaki*, and *Katsumi Kaneko**

Porous metallic solids with pore sizes of nanoscale dimensions are potentially of broad technological and fundamental interest in research areas ranging from catalysis to adsorption science. Attard and co-workers have developed some excellent approaches to preparing nanostructured metals or metal oxides by means of electrochemical deposition from the homogeneous hexagonal mesophase of non-ionic surfactants with metal salts.[1–6] This method produces mesoporous metallic thin films with arrays of uniform pore structures. Such mesoporous metallic thin films display excellent electrochemical characteristics and offer potential for many applications. Pileni and co-workers also have synthesized some nanometer-sized crystallites of metals and semiconductors using surfactant solutions, such as lamellar lyotropic liquid crystals or reverse micelles.[7,8] By using these preparation methods, a variety of metal or semiconductor particles can be produced with highly uniform shapes and sizes. Recently, Erlebacher and co-workers have prepared nanoporous gold by dealloying Ag–Au alloys.[9] The dealloying technique involves the selective dissolution of most the electrochemically active species present. As described above, research on nanoporous metals is developing in many directions, because of the ability of these materials to store high volumes of atoms, ions, or molecules, and to act as catalysts for some chemical reactions.

In this communication, we describe a synthetic route for preparing nanostructured nickel using poly(vinyl alcohol) (PVA) as a polymer precursor.[10,11] The use of PVA is significant for the formation of the metallic nickel colloids. The nickel species can be readily doped into a PVA polymer matrix in aqueous solutions. Another major advantage of the use of PVA is that the PVA can be removed almost completely by burning off. In our case, the carbon content in the final products is very slight, and can only be detected by X-ray photoelectron spectroscopy (XPS). Small amounts of carbon on nickel particles play an important part in the prevention of particle sintering. The structural properties and the adsorptive properties of the resulting compounds were also characterized by means of scanning electron microscopy (SEM), transmission electron microscopy (TEM), X-ray diffraction (XRD), X-ray absorption fine-structure (XAFS) spectroscopy, and nitrogen adsorption isotherms at 77 K.

Figure 1 shows the SEM and TEM images of the compounds which were prepared by the thermal decomposition of $Ni(OH)_2$-doped PVA films (Ni:PVA). Hereafter, the resulting compounds prepared by the thermal decomposition of Ni:PVA films are named as "Ni:PVA923." Here, the 923 in the sample name indicates the heat-treatment temperature in the thermal decomposition process. The SEM image of the product (Fig. 1a) exhibits a colloid of small nanoparticles. The TEM images (Figs. 1b,c) show the presence of fine particles. Most of the particles in the products were found to be less than 10 nm in size. Figure 2a shows the XRD patterns for Ni metal and Ni:PVA923. The powder XRD pattern of the prod-

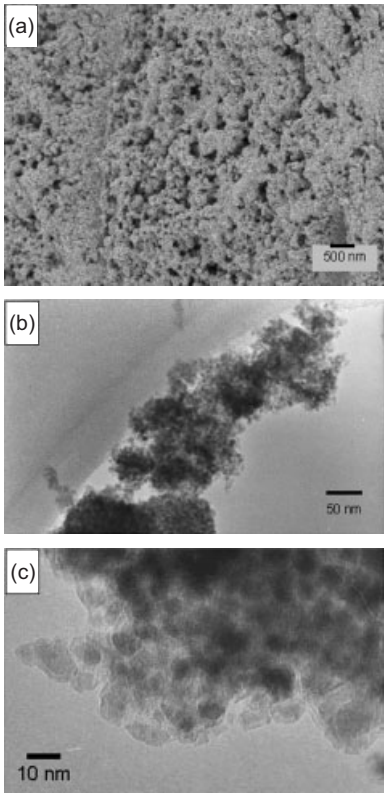

Fig. 1. The SEM and TEM images of a Ni:PVA film heat-treated at 923 K: a) SEM image, b) low-magnification TEM image, and c) high-magnification TEM image.

[*] Prof. K. Kaneko, Dr. T. Konishi, Dr. H. Kanoh
Faculty of Science, Chiba University
1-33 Yayoi, Inage, Chiba 263-8522 (Japan)
E-mail: kaneko@pchem2.s.chiba-u.ac.jp
Dr. Y. Hattori
Center for Frontier Electronics and Photonics, Chiba University
Institute of Research and Innovation
Japan Society for the Promotion Science
1-33 Yayoi, Inage, Chiba 263-8522 (Japan)
Dr. S. Kawasaki
Faculty of Textile Science and Technology, Shinshu University
3-15-1 Tokida, Ueda, Nagano 386-8567 (Japan)

[**] This work was partially supported by the Proposal-Based New Industry Creative Type Technology R & D Promotion Program (99E10-0091) from NEDO.

 © 2003 WILEY-VCH Verlag GmbH & Co. KGaA, Weinheim 0935-9648/03/0603-0529 $ 17.50+.50/0